Diffusion and Mass Transfer in Supercritical Fluids

The different behavior of fluid density and viscosity in going from the dilute gas to the dense fluid state gives rise to kinematic viscosities which, in the near supercritical region, are lower than for liquid metals. As a consequence, the relative importance of natural convection (as measured by the ratio of buyoant to inertial forces) is two orders of magnitude higher in a supercritical fluid (at constant Reynolds number) than in normal liquids.

Binary diffusion coefficients of nonvolatile solutes in supercritical fluids were measured with a technique that involved laminar flow and diffusion in a rectangular channel. The solution to this hydrodynamic problem is presented. By varying the inclination of the solute source plane with respect to the horizontal position, apparent diffusion coefficients were measured that were up to six times higher than the "true" coefficients.

Experimental binary diffusion coefficients, including published literature data, were analyzed in the light of hydrodynamic (Stokes-Einstein) theory. The analysis suggests that under the high-density, low-viscosity conditions that characterize supercritical fluids, hydrodynamic behavior at the molecular level is approached, and can be used as a basis for data extrapolation.

P. G. Debenedetti, R. C. Reid
Department of Chemical Engineering
Massachusetts Institute of Technology
Cambridge, MA 02139

Introduction

Selective dissolution of components in solids with supercritical fluids is an operation of considerable current interest. The engineering design of such a process, which generally involves contacting a packed bed of solid phase with a supercritical fluid, requires knowledge of equilibrium solubilities and component selectivities (thermodynamic constraints) as well as mass transfer rates (kinetic constraints). Most published work on such a process has concentrated on the thermodyamic aspects.

In general, one would expect the rate of dissolution to be described by relationships of the form

$$Sh = f(Re, Sc) \tag{1}$$

However, as will be discussed in detail, this simplified view is completely unacceptable in the case of supercritical fluids, and buoyant effects must be introduced through an appropriate Grashof number,

$$Sh = g(Re, Sc, Gr) \tag{2}$$

The necessity of considering natural convection effects results from the fact that supercritical fluids exhibit exceptionally small kinematic viscosities as a consequence of their high densities and low viscosities. As will be shown, buoyant effects (at constant Reynolds number) are inversely proportional to the square of the kinematic viscosity; natural convection currents are thus unusually important in supercritical fluids.

In this paper we consider diffusion and mass transfer of solids into supercritical fluids. Both theoretical and experimental considerations are treated. The experimental technique was designed to measure true diffusion coefficients (in the absence of buoyancy) as well as apparent diffusion coefficients (under the influence of arbitrarily variable free convective currents).

The current address of P. G. Debenedetti is Department of Chemical Engineering, Princeton University, Princeton, NJ 08544.

Theory

For steady laminar flow of an incompressible Newtonian fluid under the influence of gravitational forces and an imposed pressure gradient,

$$\eta\nabla^2\underset{\sim}{v} + \rho\underset{\sim}{g} - \underset{\sim}{\nabla}P = 0 \tag{3}$$

If the fluid is in contact with a surface from which a solute dissolves, the resulting concentration gradient will give rise to a density gradient that will, in turn, alter the velocity profile. This coupling between mass and momentum balances can be treated in an approximate manner for those cases where concentration (and density) changes are small by expanding the density about the pure fluid value in terms of solute concentration in a Taylor series, truncating after the linear term, and neglecting the concentration dependence of other physical properties,

$$\rho = \rho_o + \left(\frac{\partial\rho}{\partial c}\right)_{T,P,c_o}(c - c_o) = \rho_o[1 - \beta_m(c - c_o)] \tag{4}$$

Substituting Eq. 4 into Eq. 3 leads to

$$\eta\nabla^2\underset{\sim}{v} + \rho_o\underset{\sim}{g}[1 - \beta_m c] - \underset{\sim}{\nabla}P = 0 \tag{5}$$

where $c_o = 0$ has been assumed.

Equation 5 (Boussinesq's approximation) is valid only for small concentration gradients. To illustrate, let us apply it to flow in a conduit of radius R, and at the same time nondimensionalize it by defining

$$\Pi = P + \rho_o g h \tag{6}$$

$$\Pi^+ = \Pi/\rho_o\langle v\rangle^2 \tag{7}$$

$$v^+ = v/\langle v\rangle \tag{8}$$

$$r = c/c_i \tag{9}$$

where $\langle v\rangle$ is the average fluid velocity in the duct, c_i is the solute concentration at the duct boundary where phase equilibrium is assumed, and h is the relative height of a plane of constant hydrostatic pressure, measured along the direction of gravity

$$\underset{\sim}{\nabla}h = -\underset{\sim}{g}/|\underset{\sim}{g}| \equiv -\underset{\sim}{g}^o \tag{10}$$

Substituting Eqs. 6 through 10 into Eq. 5, and nondimensionalizing,

$$\frac{2}{Re}(\nabla^+)^2 e^+ - \underset{\sim}{\nabla}^+\Pi^+ - \underset{\sim}{g}^o\left(\frac{Gr}{Re^2}\right)\left(\frac{r}{2}\right) = 0 \tag{11}$$

In Eq. 11 the duct radius R has been used as the length scale. Defining $\Delta\rho$ as the difference in fluid density at the solid interface and in the bulk, $\rho_i - \rho_o$, we can place a physical interpretation on the important ratio Gr/Re^2. That is, noting that

$$\text{Buoyant forces} \sim 2Rg\Delta\rho \tag{12}$$

$$\text{Viscous forces} \sim \eta\langle v\rangle/2R \tag{13}$$

$$\text{Inertial forces} \sim \langle v\rangle^2\rho_o \tag{14}$$

then

$$\frac{Gr}{Re^2} = \left[\frac{(2Rg\Delta\rho)(\langle v\rangle^2\rho_o)/(\eta\langle v\rangle/2R)^2}{[\langle v\rangle^2\rho_o]^2/(\eta\langle v\rangle/2R)^2}\right] = \frac{2Rg\Delta\rho}{\langle v\rangle^2\rho_o} = \frac{\text{Buoyant forces}}{\text{Inertial forces}} \tag{15}$$

The ratio Gr/Re^2 can be used to investigate the relative importance of natural convection, as follows: if different fluids were to flow inside similar conduits under diffusive mass transfer conditions, then at any given Reynolds number, and assuming comparable density changes $\Delta\rho/\rho_o$, the relative importance of natural convection is inversely proportional to the square of the kinematic viscosity of the fluid in question.

The significance of this deduction lies in the fact that the kinematic viscosities of supercritical fluids are very small, and therefore the role of buyoancy forces is often predominant in mass transfer problems involving such fluids.

Figure 1 is a graph of the density, viscosity, and kinematic viscosity of CO_2 at 310 K ($Tr = 1.02$). For this material the critical pressure is 73.8 bar. The density of CO_2 at supercritical conditions ($Tr > 1$, $Pr > 1$) is close to that of normal liquids, whereas the viscosity is only a factor of six greater than for a low-pressure gas. As can be seen from Figure 1, this different behavior is due to the fact that whereas low-pressure gases are compressible, their viscosity is virtually pressure-independent. The kinematic viscosity of a supercritical fluid is then remarkably small ($\sim 8 \times 10^{-8}$ m^2/s for CO_2 in Figure 1).

In Figure 2 we compare the properties of air, water, and mer-

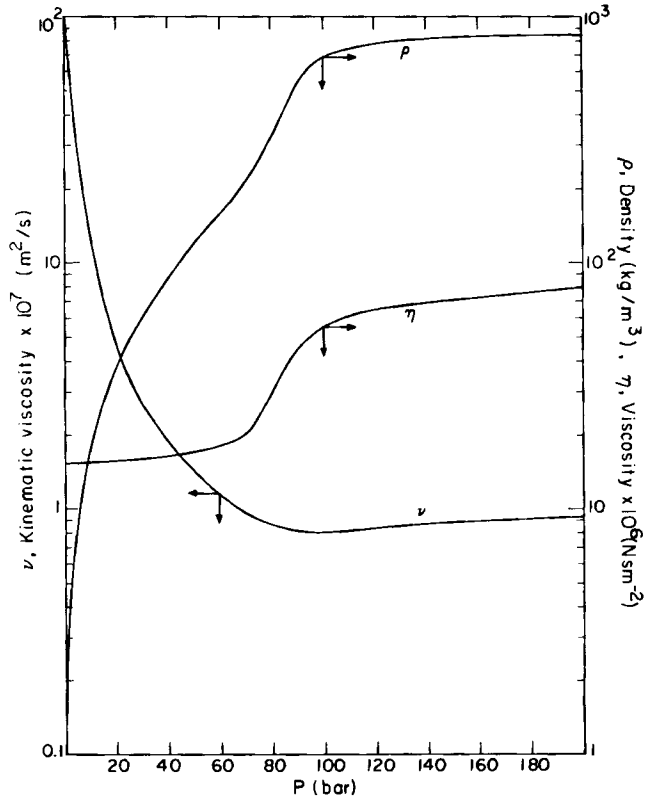

Figure 1. Density, viscosity, and kinematic viscosity of CO_2 at 310 K.

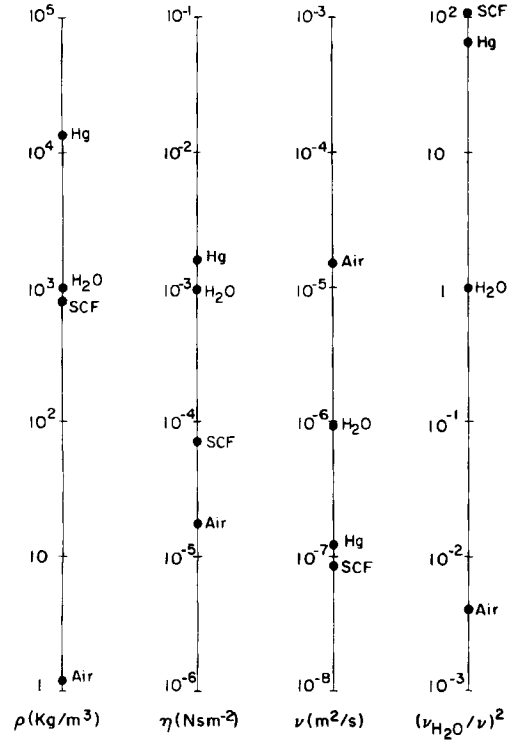

Figure 2. Comparison of physical properties of air, water, mercury, and CO_2, showing relative importance of natural convection at constant Reynolds numbers.

Air, H_2O, Hg at 298 K and 1 bar; CO_2 at 310 K and 150 bar.

cury at 298 K and 1 bar with those of supercritical CO_2 at 150 bar and 310 K. We note the fact that, for ν, CO_2 has the lowest value (lower than for mercury, a liquid metal). The relative importance of buoyant forces at constant Reynolds number (scaled with the corresponding value for water) is therefore more than two orders of magnitude higher in a supercritical fluid than in normal liquids—Figure 2, last column.

This phenomenon is unrelated to the free convective currents that originate very close to criticality as a consequence of the diverging fluid compressibility.

Flow Regimes

The extent to which natural convection controls the overall transport mechanism in a supercritical fluid (SCF) is best illustrated in the case of vertical flow inside cylindrical ducts.

Figure 3, adapted to mass transfer from heat transfer theory (Metais and Eckert, 1964; Eckert and Drake, 1972) shows the possible regimes that can exist for vertical flow inside a cylinder under the combined influence of buoyant forces and pressure gradients. This figure summarizes available experimental data and theoretical predictions, and covers the cases of forced and free convection both aiding and opposing each other. The diagram is valid for $0.01 < Sc\ D/L < 1$.

A necessary, but not sufficient, condition for forced laminar flow is $Ra\ D/L < 10^4$. This criterion has been used in Figure 4, where the area lying above and to the right of each curve represents geometries for which laminar flow is unattainable in SCF operation (notice the ν and Sc values). The parameter in Figure 4 is the relative density change. Thus it can be seen that even for

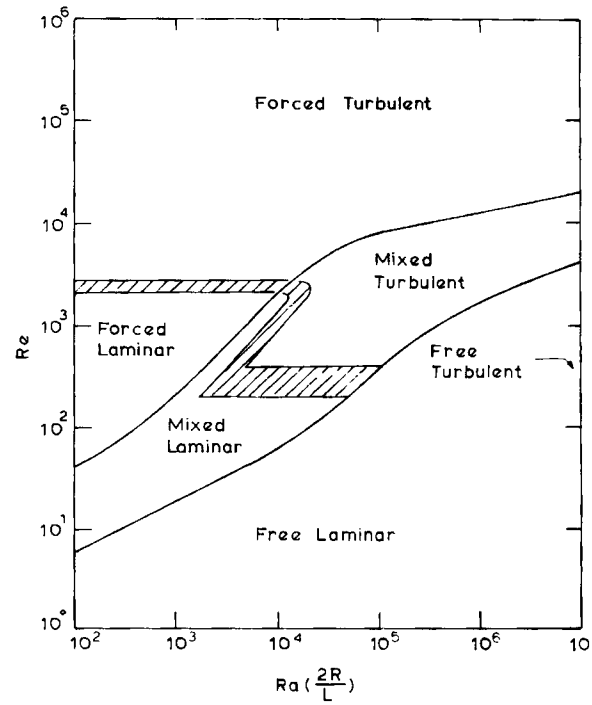

Figure 3. Hydrodynamic regimes for vertical cylindrical duct flow.

negligibly small density changes (10^{-3}) and aspect ratios (10^{-3}), forced laminar flow cannot be attained for $D > 8$ mm. The curves are shown as broken lines for $D/L > 10^{-1}$ since, for $Sc = 10$, this is the upper limit for the validity of Figure 3.

For packed bed flow, the large contribution of buoyant forces suggests that the usual mass transfer correlations are unsuitable for design purposes when supercritical fluids are involved if the

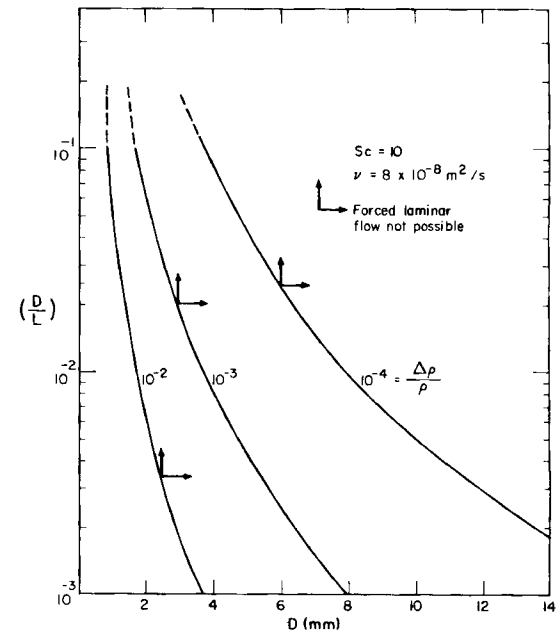

Figure 4. Cylindrical duct geometries for which forced, vertical laminar flow is impossible under supercritical conditions due to natural convection.

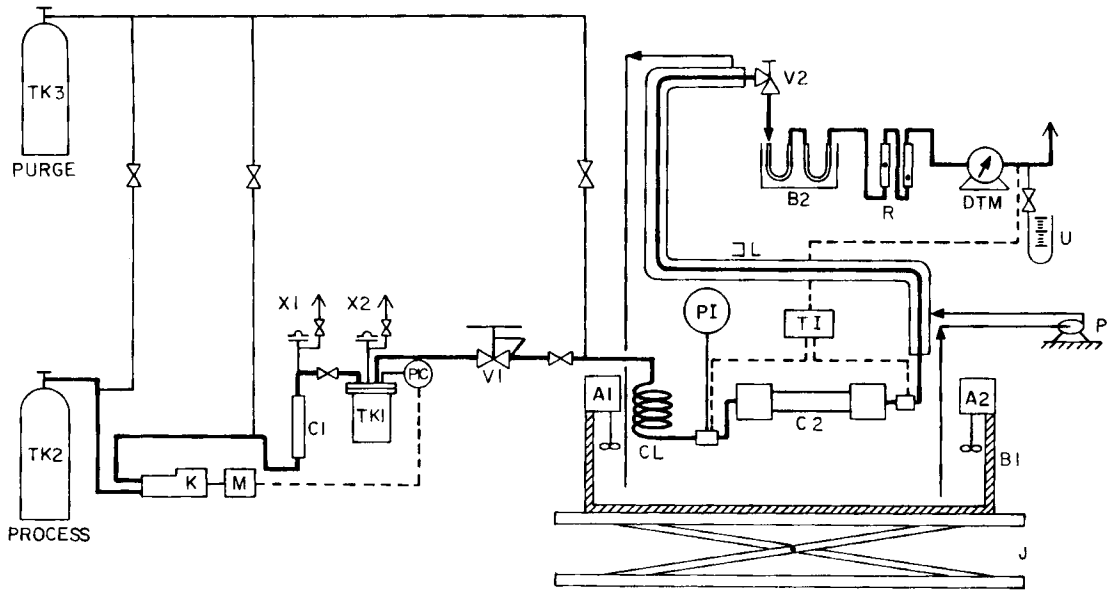

Figure 5. Equipment flow sheet.

controlling resistance is in the supercritical phase. Correlations that take into account buoyant forces have been published (Karabelas et al., 1971), but these do not cover the low Schmidt number range characteristic of SCF's.

To investigate the actual sensitivity of mass transfer in supercritical fluids to natural convection effects, experiments were conducted as described below.

Apparatus and Experimental Procedure

A schematic flow sheet of the experimental apparatus is shown in Figure 5. The solvent gas is compressed by diaphragm compressor *K* (Aminco J46-13411) and pumped from *TK2* to a 2 L autoclave, *TK1*, whose pressure is maintained by an on-off controller (indicator-controller *PIC*) acting on the compressor's electric drive *M*. A pressure regulator, *V1* (Matheson model 4 high-pressure regulator), eliminates downstream pulsations.

The pressurized solvent is preheated to the desired temperature in coil *CL*, which is immersed in a water bath, *B1*, whose temperature is maintained by heater-circulators *A1* and *A2* (Thermomix 1460, accurate to within 0.01°C). The pressure is displayed on a panel-mounted gauge, *PI* (Heise gauge, 0–400 bar, accurate to 0.5 bar). *C2*, the diffusion tube, is a 5 cm × 32 cm stainless steel pipe inside of which is located a flat plate where the diffusional process occurs.

The partially saturated fluid emerges from *C2* and flows through a jacketed line (*JL*) up to valve *V2*. Bath water is circulated through the jacket by pump *P* to maintain the outlet line isothermal and prevent solute precipitation. *V2* (30 VM 4082, GA, Autoclave Engineers) is a 0.8 cm (¼ in) regulating valve that controls the flow and reduces the pressure to atmospheric. In operation, it is maintained at least 20°C above the solute's melting point in order to avoid clogging due to solid accumulation.

The precipated solute is collected in two packed U-tubes immersed in an ice bath *B2*; the solvent flows through rotameters *R*; the total flow is then determined from the dry test meter (*DTM*) reading.

The actual experiment involves fully developed laminar flow of a supercritical fluid inside a horizontal rectangular channel, Figure 6, the bottom surface of which is coated with the solute of interest. A brass plate (*4*) is tightly fitted into a machined enclosure made up of two aluminum hemicylinders (*1*, *2*); fluid then passes through the resulting 2.5 cm × 0.3 cm (1 in × ⅛ in) rectangular channel (*3*). The plate contains three sections: a sec-

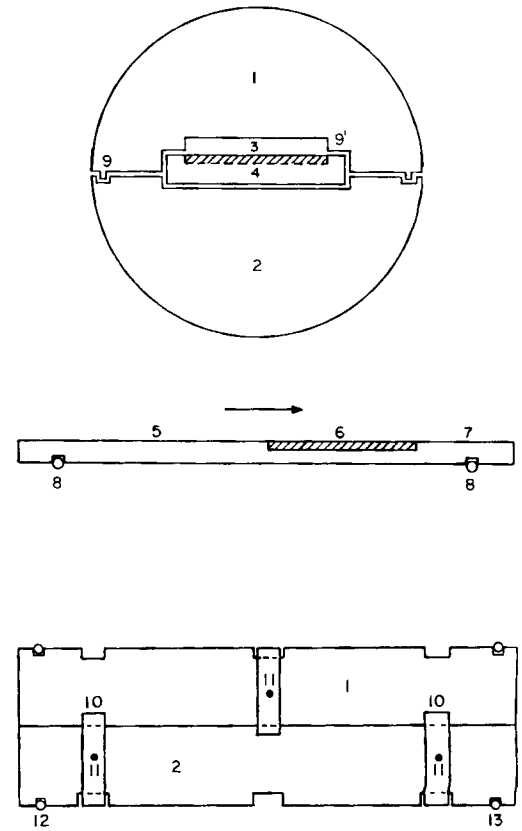

Figure 6. Flat plate assembly for hydrodynamic experiments.

tion (5) where laminar flow is allowed to develop, a test section (6), and an outlet section (7). The test section is made by casting molten solute into a recess and polishing the surface flat after solidification.

The hemicylinders are held together by three nut-tightened straps (*10, 11*); the mating surface (*9*) is machined so as to provide a labyrinth seal, the space between the two surfaces being sealed with Teflon tape. Cord stock (*8*) forces the flat plate against the upper surface (*9'*) and prevents fluid from bypassing the test section.

The whole assembly is tightly fitted inside *C2*. Sealing is provided by O-ring *13*, while O-ring *12* is notched: the pressure in *3* is thus equal to the pressure outside *1* and *2*.

When channel *3* is horizontal, the flow is unaffected by gravity since the heavier (saturated) fluid at the interface is always at the bottom of the channel (see the Discussion section, however, for possible exceptions). Binary diffusion coefficients can then be measured by weighing the evaporated solute trapped in *B2* after precipitating from a measured quantity of solvent while operating at steady state (constant flow rate) in a carefully timed experiment. The governing equations are developed below.

Variable buoyant effects can be introduced by rotating *1* and *2* inside *C2*; thus, when *3* is not horizontal, the same experiment should give rise to different results. In this way, information can be gathered on the relative importance of natural convection in SCF's.

Diffusive Transport in Rectangular Ducts

For fully developed laminar flow of an incompressible Newtonian fluid in a rectangular duct of width $2a$ and height $2b$, the velocity profile can be expressed as (Shah and London, 1978)

$$\frac{v}{v_{max}} = \left[1 - \left(\frac{|y|}{b}\right)^n\right]\left[1 - \left(\frac{|z|}{a}\right)^m\right] \tag{16}$$

where flow is in the x direction, and $-b \le y \le b$, $-a \le z \le a$. n and m were obtained by matching a finite-difference solution of the momentum balance equation to Eq. 16.

$$m = 1.7 + 0.5\alpha^{-1.4} \tag{17}$$

$$n = \begin{cases} 2 & \alpha \le 1/3 \\ 2 + 0.3(\alpha - 1/3) & \alpha \ge 1/3 \end{cases} \tag{18}$$

$$\alpha = b/a \tag{19}$$

Figure 7 shows several (v/v_{max}) curves, plotted according to Eqs. 16–18, with $\alpha = 1/3$.

For steady state diffusion of a solute,

$$v\frac{\partial c}{\partial x} = \mathcal{D}\nabla^2 c \tag{20}$$

Combining Eqs. 16 and 20 we obtain an expression that can be nondimensionalized by defining

$$\beta = L/2a = L\alpha/2b \tag{21}$$

$$x^+ = x/b \tag{22}$$

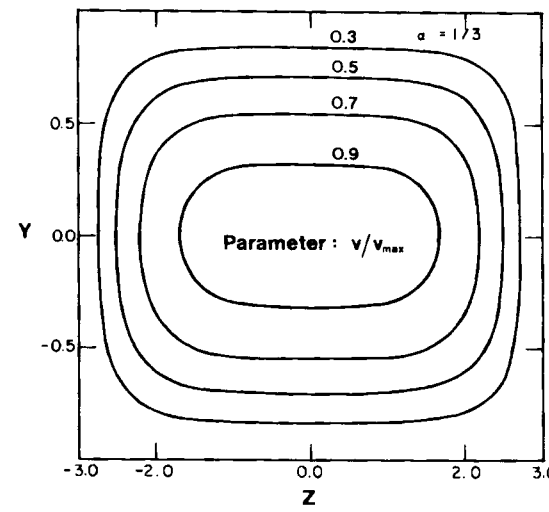

Figure 7. Velocity profiles as per Eqs. 16, 17, and 18; $\alpha = 1/3$.

$$y^+ = y/b \tag{23}$$

$$z^+ = z/b \tag{24}$$

$$c^+ = (c - c_i)/(c_o - c_i) \tag{25}$$

$$v^+ = v/\langle v\rangle \tag{26}$$

where L is the coated length (7.62 cm in our case). It can be shown (Debenedetti, 1984) that upon nondimensionalization we obtain the following scales,

$$\text{Convection } (x) \sim (\alpha/2\beta) \sim 2 \times 10^{-2}{:}1 \tag{27}$$

$$\text{Diffusion } (y) \sim (2\beta/\alpha Pe) \sim 5 \times 10^{-3}{:}1/4 \tag{28}$$

$$\text{Diffusion } (x) \sim (\alpha/2\beta Pe) \sim 2 \times 10^{-6}{:}10^{-4} \tag{29}$$

$$\text{Diffusion } (z) \sim (2\beta\alpha/Pe) \sim 8 \times 10^{-5}{:}4 \times 10^{-3} \tag{30}$$

where the axial Peclet number is defined as

$$Pe = \langle v\rangle L/\mathcal{D} \tag{31}$$

and we have used $\alpha = 1/8$, $\beta = 3$, and $Pe = 10^4$ ($\langle v\rangle \sim 1.3 \times 10^{-3}$ m/s; $\mathcal{D} \sim 10^{-4}$ cm^2/s), the latter two values corresponding in the present case to typical axial velocities and diffusion coefficients, respectively.

The equation to be solved therefore can be written as

$$(2\zeta^+ - \zeta^{+2})\frac{\partial c^+}{\partial x^+} = A'(z^+)\frac{\partial^2 c^+}{\partial \zeta^{+2}} \tag{32}$$

where

$$\zeta = b - y \tag{33}$$

$$A'(z^+) = \frac{4\beta}{3\alpha Pe}\left(\frac{m}{m+1}\right)[1 - (\alpha|z^+|)^m]^{-1} \tag{34}$$

The boundary conditions corresponding to an equilibrium solute-coated surface at $y = -b$ ($\zeta = 2b$), and pure solvent at $x = 0$, are

$$c^+(x^+, 2) = 0 \tag{35}$$

$$\left(\frac{\partial c^+}{\partial \zeta^+}\right)_{(x^+, o)} = 0 \tag{36}$$

$$c^+(o, \zeta^+) = 1 \tag{37}$$

Solving Eq. 32, subject to Eqs. 35–37, the following expressions result for the local Sherwood number and cup-average relative saturation:

$$Sh(\alpha, x^+) = \frac{-16m}{3(m+1)(1+\alpha)} \cdot \frac{\sum_{n=1}^{\infty} B_n \cdot E_n \cdot \psi_n(Gz', m)}{\sum_{n=1}^{\infty} A_n \cdot \Phi_n(Gz', m)} \tag{38}$$

$$\langle r(\alpha, x^+)\rangle = 1 + \frac{3(m+1)}{2m} \sum_{n=1}^{\infty} A_n \cdot \Phi_n(Gz', m) \tag{39}$$

where Sh is a z-averaged local Sherwood number, with 4 (Area/Perimeter) as characteristic length,

$$Sh(x^+) = \frac{4b}{(1+\alpha)\mathcal{D}} \int_0^1 k\, d(z/a) = -\frac{4}{1+\alpha} \cdot \frac{1}{\langle c^+\rangle} \int_0^1 \left(\frac{\partial c^+}{\partial \zeta^+}\right)_{(\zeta^+=2)} d(z/a) \tag{40}$$

and

$$\langle c^+\rangle = 1 - \langle r\rangle = \frac{1}{4ab} \int\int v^+ c^+ \, ds \tag{41}$$

Gz' is a modified Graetz number,

$$Gz' = \frac{x\mathcal{D}}{\langle v\rangle b^2} \tag{42}$$

and ϕ_n, ψ_n, A_n, B_n, and E_n are defined in the Appendix, where tabulated values of A_n, B_n, and E_n ($n = 1, \ldots, 5$) are also given.

Figures 8 and 9 are plots of Eqs. 38 and 39. As can be seen, for a given aspect ratio α, the relative saturation is a function of Gz'. For a given coated length x and flow rate $\langle v\rangle$, the measured relative saturation is then only a function of the diffusion coefficient.

It follows from this discussion that the calculation of binary diffusion coefficients requires knowledge of the equilibrium solubility of the solute in the solvent under experimental conditions. Thus, for each experiment an independent measurement of equilibrium solubility at the given T and P must be performed. This was done in the present case using a flow technique

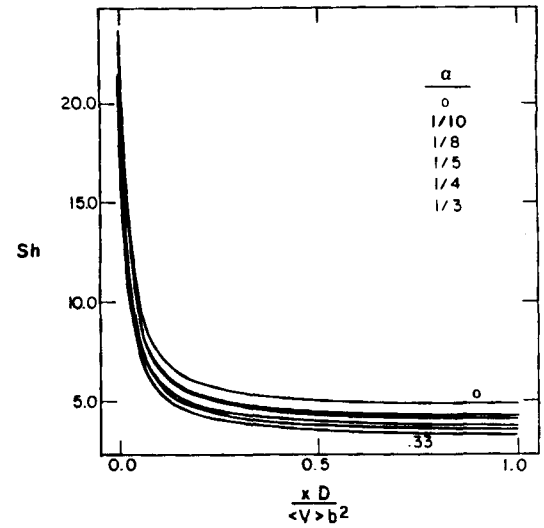

Figure 8. z-averaged local Sherwood number as a function of Gz' for various aspect ratios.

that has been applied successfully to the study of solubilities of nonvolatile solutes in supercritical fluids (Kurnik, 1981; Kurnik et al., 1981; Kurnik and Reid, 1981; Schmitt and Reid, 1986).

Results

Using the experimental and analytical methods explained above, we studied diffusion coefficients in four binary systems: naphthalene-SF_6, benzoic acid-SF_6, benzoic acid-CO_2, and 2-naphthol-CO_2. The results are summarized in Table 1. The measured diffusion coefficients are shown in Figure 10 as a function of solvent density, and in Figure 11 as a function of solvent reduced pressure. The reported diffusion coefficients are valid to within a conservatively estimated ±22% relative error. (A detailed discussion of experimental errors is available as supplementary material.)

The experimentally controlled variables were temperature and pressure; solvent densities were obtained via the Peng-Robinson equation of state for SF_6 (Peng and Robinson, 1976), and from the *International Thermodynamic Tables of the Fluid State* (Angus et al., 1976) for CO_2. The approximation whereby

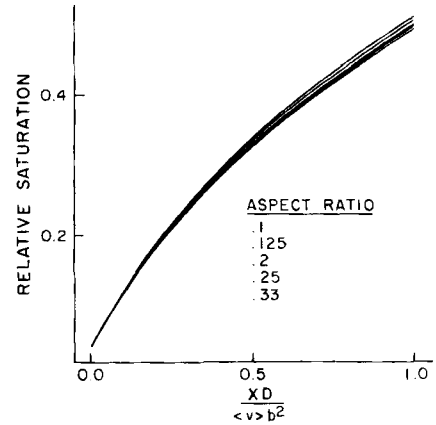

Figure 9. Relative saturation as a function of Gz' for various aspect ratios.

Table 1. Experimentally Measured Diffusion Coefficients

Solute	Solvent	T K	P bar	$10^{-3}\rho^*$ mol/m³	$10^5\mathcal{D}$ cm²/s
Benzoic acid	SF_6	328.2	65	7.59	9.26
		328.2	80	8.37	8.61
		328.2	120	9.59	7.02
		338.2	65	6.28	13.40
		338.2	80	7.42	10.70
		338.2	120	8.95	8.15
Naphthalene	SF_6	318.2	65	8.69	8.85
		318.2	80	9.24	8.33
		318.2	120	10.20	6.80
		328.2	65	7.59	13.80
		328.2	80	8.37	11.70
Benzoic acid	CO_2	318.2	160	17.16	4.90
		318.2	200	18.48	4.27
		328.2	160	15.25	9.14
		328.2	200	17.16	6.83
2-Naphthol	CO_2	308.2	150	18.52	7.03
		308.2	200	19.69	6.63
		308.2	250	20.50	6.45
		318.2	165	17.31	7.43
		318.2	250	19.50	7.00

*SF_6 density from Peng-Robinson equation of state (Peng and Robinson, 1976)
CO_2 density from IUPAC tables (Angus et al., 1976)

fluid density is calculated without taking into account solute concentration is only justified for dilute systems. The maximum solute weight fractions under experimental conditions were extremely low, as shown below:

	% Wt. Frac.	Temp., K	Press., bar
Benzoic acid in SF_6	0.02	338	120
Naphthalene in SF_6	0.34	328	120
Benzoic acid in CO_2	1.06	328	200
2-Naphthol in CO_2	0.28	318	250

Under these conditions the infinite dilution assumption introduces no analytically detectable error.

At constant temperature, low density diffusion coefficients are inversely proportional to fluid density. This result can be derived theoretically (Chapman and Cowling, 1970). Furthermore, since the pressure and density of an ideal gas are directly proportional at constant temperature, a logarithmic plot of diffusion coefficients vs. pressure approaches a limiting slope of -1 at low densities (Paulaitis et al., 1983). No equivalent simple relationship exists at high pressure, and the use of a semilog scale in Figure 11 is simply a matter of convenience. Similarly, there exists no accurate theory that will predict the isothermal density dependence of diffusion coefficients in dense fluids. The linear relationship that results when data from these systems are plotted in log D vs. ρ coordinates (Debenedetti, 1984) has been reported by other researchers who studied diffusion in supercritical fluids (Swaid and Schneider, 1979; Feist and Schneider, 1982). However, in the present case as well as in the above-mentioned studies the ratio of maximum to minimum density for any given isotherm was at most three; the observed linearity should therefore be interpreted with caution.

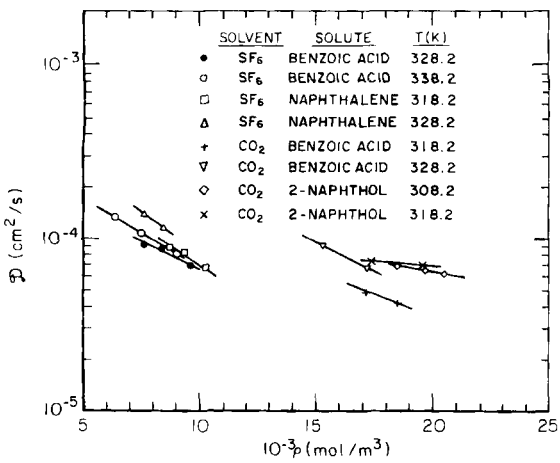

Figure 10. Experimental diffusion coefficients as a function of solvent density.

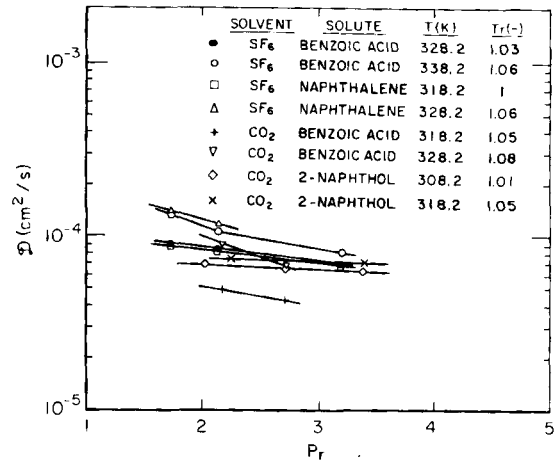

Figure 11. Experimental diffusion coefficients as a function of solvent reduced pressure.

Discussion

At any given density the measured diffusion coefficients of benzoic acid are lower (within experimental accuracy) than those of naphthalene (in SF_6) and 2-naphthol (in CO_2), both of which are larger molecules than benzoic acid. This suggests fluid phase association of benzoic acid, a behavior experimentally observed in liquid CCl_4 and $CHCl_3$ (I'Haya and Shibuya, 1965) and in its own vapor, C_6H_{12}, CCl_4, and C_6H_6 (Allen et al., 1966). That this phenomenon can indeed be quantitatively significant even at low benzoic acid concentrations can be seen from the calculated values (Debenedetti, 1984) for the unassociated $(1 - x)$ and associated $(x/2)$ fractions that follow from the reported association constants for benzoic acid in CCl_4 (Allen et al., 1966): 31% unassociated, 34.5% associated at 303 K; 61.9% unassociated, 19.05% associated at 333 K, both for a total benzoic acid concentration (7×10^{-1} mol/m³) that is representative of actual experimental conditions.

We note, furthermore, the pronounced temperature dependence of the measured diffusion coefficients of benzoic acid in CO_2. Although the postulated dimerization has not been measured in CO_2, an effective activation energy for diffusion can be obtained from the two coefficients measured at the same density and two different temperatures (318 K, 328 K, $\rho_r = 1.61$). This value (28.9 kJ/mol) is in good qualitative agreement with the

experimentally measured activation energies for the dimerization of benzoic acid in C_6H_{12} (26.8 kJ/mol), CCl_4 (23 kJ/mol), and in its own vapor phase (33.9 kJ/mol) (Allen et al., 1966). The overall diffusion coefficient, however, is related in a nonlinear way to the dimerization constant, so the above considerations should only be taken qualitatively.

The temperature dependence of the measured diffusion coefficients is interesting, since it provides useful insights into dense fluid behavior. Hard sphere theory (Dymond, 1974) or its ad hoc modification, rough hard sphere theory (Chandler, 1975), predicts a $T^{1/2}$ dependence of diffusion coefficients at constant density (slightly modified in rough hard sphere theory by allowing for a mild temperature dependence of the sphere's diameter). In a hydrodynamic approach, on the other hand, the Stokes-Einstein expression is used as a starting point

$$\mathcal{D} = \frac{kT}{6\pi a\eta} \tag{43}$$

where $\mathcal{D}$ is the diffusion coefficient of a Brownian sphere of radius a in a continuum of viscosity η and temperature T, when no slip exists between the particle and the continuum. Since the viscosity of liquids is a very strongly decreasing function of temperature, often correlated in the Andrade form (Andrade, 1930)

$$\eta = A \exp(B/T) \tag{44}$$

it follows that diffusion coefficients in dense fluids should, according to this approach, exhibit a stronger temperature dependence than predicted by hard sphere theories.

It is important to point out that the hydrodynamic limit—i.e., Eq. 43—can also be obtained in principle from hard sphere theory, according to which (Dymond, 1974)

$$\mathcal{D} \sim T^{1/2}(V - 1.384V_o)\sigma^{-2} \tag{45}$$

$$\eta \sim T^{1/2}(V - 1.384V_o)^{-1}\sigma \tag{46}$$

where V_o is the hard sphere close-packed molar volume, V the molar volume, and σ, the hard sphere diameter. From Eqs. 45 and 46 we readily obtain

$$\mathcal{D}\eta T^{-1} \sim \sigma^{-1} \tag{47}$$

in agreement with the Stokes-Einstein equation. The temperature dependence of fluid viscosity predicted by Eq. 46, however, is obviously inconsistent with experimental evidence for dense fluids, Eq. 44. To remedy this, temperature-dependent hard sphere diameters have been regressed from experimental data (Fury et al., 1979; Chen, 1983).

The Stokes-Einstein equation can be rewritten as

$$\frac{\eta\mathcal{D}}{kT} = \frac{1}{6\pi a} \tag{48}$$

where the quantities on the lefthand side are experimentally measurable. Regardless of the validity of the no-slip assumption (and hence of the coefficient 6π), and of the meaning of a for the solutes considered here, it is of interest to investigate the behavior of the quantity $\eta\mathcal{D}T^{-1}$.

Table 2. Stokes-Einstein Analysis

Solute	Solvent	T K	P bar	$10^7\eta^*$ Ns/m^2	$10^{16}\eta\mathcal{D}T^{-1}$ N/K
Benzoic acid	SF_6	328.2	65	633.65	17.88[a]
		328.2	80	733.70	19.35
		328.2	120	934.63	19.99
		338.2	65	504.65	19.99
		338.2	80	624.12	19.75
		338.2	120	823.34	19.84
Naphthalene	SF_6	318.2	65	775.25	21.56[b]
		318.2	80	864.11	22.62
		318.2	120	1172.22	25.05
		328.2	65	633.65	26.64
		328.2	80	737.70	26.30
Benzoic acid	CO_2	318.2	160	629.05	9.69
		318.2	200	709.17	9.52
		328.2	160	540.32	15.05
		328.2	200	633.56	13.18
2-Naphthol	CO_2	308.2	150	704.61	16.07[c]
		308.2	200	784.16	16.87
		308.2	250	852.16	17.83
		318.2	165	641.42	14.98
		318.2	250	773.22	17.01

*Calculated from Jossi et al. (1962); low-pressure viscosity from Eqs. 9-3.9, 9-4.3, and Appendix C of Reid et al. (1977).
[a]Standard deviation 4.17% of mean.
[b]Standard deviation 9.20% of mean.
[c]Standard deviation 6.50% of mean.

Table 2 shows the behavior of $\eta\mathcal{D}T^{-1}$ for the systems that we investigated experimentally. For SF_6 as a solvent ($1.24 < \rho_r < 2.1$), both systems exhibit fairly constant $\eta\mathcal{D}T^{-1}$ values, suggesting that hydrodynamic arguments may be relevant. We note, in particular, that the $\eta\mathcal{D}T^{-1}$ value for benzoic acid is lower than for naphthalene, again suggesting fluid phase association of benzoic acid. The pronounced temperature dependence of the benzoic acid-CO_2 $\eta\mathcal{D}T^{-1}$ values in Table 2 is consistent with an exothermic dimerization, giving rise to a smaller effective size at higher temperatures.

It follows from Eq. 43 that a plot $\mathcal{D}$ vs. $T\eta^{-1}$ should, for any given system exhibiting hydrodynamic behavior at the molecular level, yield a single straight line through the origin. Alternatively, we can plot $\mathcal{D}$ vs. η^{-1} (fluidity): for hydrodynamic behavior the data should fall on straight lines through the origin, with slopes proportional to T (for a given system).

Feist and Schneider (1982) analyzed diffusion coefficients of benzene, phenol, naphthalene, and caffeine in supercritical CO_2 at 40°C and, from a $\mathcal{D}$ vs. η^{-1} plot concluded that the Stokes-Einstein equation did not apply, since the intercepts were nonzero. Feist and Schneider correlated their data with a power law relationship $\mathcal{D}$ vs. η^{-a} ($0 < a < 1$), as proposed by Hayduck and Cheng (1971).

Figure 12 is a plot of the SF_6–benzoic acid data obtained in this work in $\mathcal{D}$ vs. $T\eta^{-1}$ coordinates. As can be seen, the plot is linear to a good approximation, but the extrapolated line yields a small but finite intercept. The general picture that emerges is summarized in Figure 13. Hydrodynamic behavior is approached at high viscosities; deviations from this limiting behavior can be correlated (but not understood) by means of empirical power law relationships of the type $\mathcal{D}$ vs. η^{-a}. Supercritical vis-

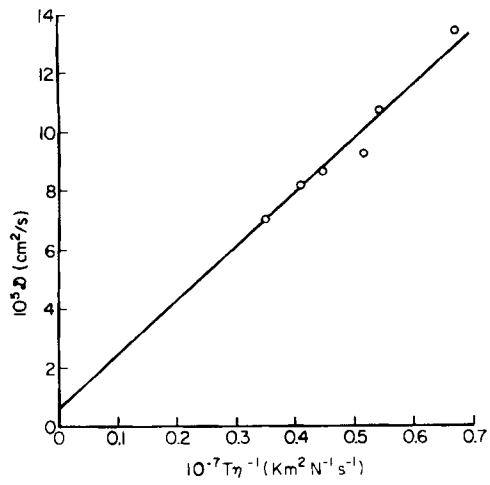

Figure 12. Benzoic acid–SF_6 data plotted in Stokes-Einstein fashion.

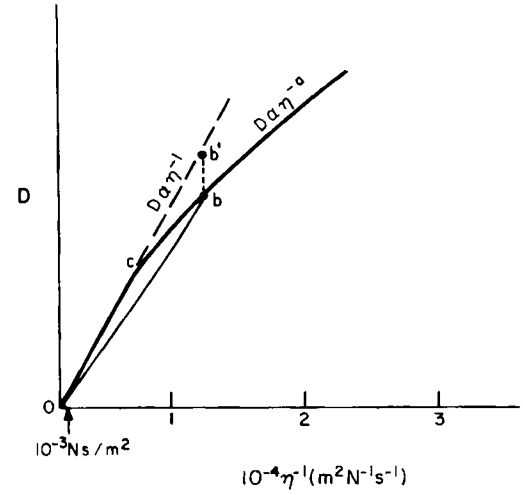

Figure 13. Hydrodynamic and power law behavior of infinite dilution binary diffusion coefficient as a function of fluidity.

cosities fall roughly in the range $4 \times 10^{-5} \leq \eta \leq 10^{-4}$ Ns/m² for $1.1 \leq Pr \leq 4$ and $1 \leq Tr \leq 1.06$, which corresponds to $1 \leq 10^{-4}\ \eta^{-1} \leq 2.5$ in the fluidity scale of Figure 13; a typical liquid viscosity is also shown for comparison. The exact point at which hydrodynamic behavior breaks down (point *c*) cannot at present be predicted from first principles. However, we can conclude from the figure that predictive correlations based on the Stokes-Einstein equation (Wilke and Chang, 1955; Scheibel, 1954; Reddy and Doraiswamy, 1967; Lusis and Ratcliff, 1968) will overestimate diffusion coefficients in supercritical fluids. In addition, for high viscosities (or, equivalently, for high pressures any given temperature), the quantity $\eta\mathcal{D}T^{-1}$ approaches a constant value; geometrically, this is equivalent to saying that at small fluidity values the curve *Ocb* is well approximated by the line *Ob*. As an example, the measured diffusion coefficients of benzene in supercritical CO_2 (Swaid and Schneider, 1979) give rise to an $\eta\mathcal{D}T^{-1}$ value that is constant to within a 4.6% standard deviation when $\eta \geq 4 \times 0^{-5}$ Ns/m², irrespective of *T* and *P*. At high enough viscosities, hydrodynamic behavior is approached, and this fact can be used to extrapolate experimental data by assuming constancy of $\eta\mathcal{D}T^{-1}$.

To test the above conclusions regarding the applicability of Stokes-Einstein-based correlations to diffusion in supercritical fluids, we applied the Wilke-Chang, Scheibel, Reddy-Doraiswamy, and Lusis-Ratcliff correlations to three of the four systems investigated, as well as to the CO_2-benzene ($308 \leq T \leq 328$ K; $80 \leq P \leq 160$ bar [Swaid and Schneider, 1979]), CO_2-naphthalene ($308 \leq T \leq 328$ K; $83 \leq P \leq 304$ bar [Iomtev and Tsekhanskaya, 1964]), and C_2H_4-naphthalene systems ($285 \leq T \leq 308$ K; $66 \leq P \leq 304$ bar [Iomtev and Tsekhanskaya, 1964]). The results are summarized in Table 3, where the first four columns are average ratios of predicted to measured diffusion coefficients (average, in this case, signifies that this ratio was calculated for all of the experimentally measured coefficients, and then averaged). The fifth column in Table 3 is the mean of the experimental $\eta\mathcal{D}T^{-1}$ values, and the sixth column is the corresponding standard deviation, in percent of the mean. Although the standard deviations are quite small, the constancy of $\eta\mathcal{D}T^{-1}$ invariably improved away from the solvent's critical point. All correlations were used with ϕ (association factor) equal to 1. Details of these calculations are provided elsewhere (Debenedetti, 1984).

As anticipated, all correlations overpredict observed diffusion coefficients by a considerable amount, with the single exception of the Wilke-Chang expression for the ethylene-naphthalene system. For diffusion in CO_2, the Wilke-Chang expression is consistently less in error.

At present, no reliable predictive method exists for the calculation of diffusion coefficients in supercritical fluids. If one experimental value of $\mathcal{D}$ is available, it can be used to estimate diffusion coefficients in the same system under different conditions by assuming a constant $\eta\mathcal{D}T^{-1}$ value. This method is not recommended for $\eta < 4 \times 10^{-5}$ Ns/m².

Table 3. Average Values of Ratios Between Predicted and Experimental Diffusion Coefficients for Various Hydrodynamic Correlations

System	Wilke-Chang	Scheibel	Reddy-Doraiswamy	Lusis-Ratcliff	$\langle 10^{16}\eta\mathcal{D}T^{-1}*\rangle$	Std.** Dev.
Benzoic acid–SF_6	2.50	1.79	3.01	1.80	19.47	4.17
Naphthalene–SF_6	1.78	1.34	2.25	1.29	24.43	9.20
2-Naphthol–CO_2	1.44	1.60	2.33	1.68	16.55	6.50
Benzene–CO_2	1.23	1.41	1.47	1.36	26.50	9.40
Naphthalene–CO_2	1.33	1.48	2.15	1.55	18.16	12.90
Naphthalene–C_2H_4	0.884	1.36	1.29	1.36	21.41	6.35

*Mean of experimental values, in N/K
**Standard deviation, in percent of mean value

Effect of Natural Convection

The importance of natural convection in the overall mechanism of mass transfer with supercritical fluids has already been discussed. Buoyant effects can be introduced by performing the hydrodynamic experiments with the two hemicylinders, Figure 6, rotated at an angle α with respect to the horizontal inside the high-pressure steel enclosure.

Before discussing the results of such experiments, the criteria for the development of stable and unstable density profiles will be analyzed. In the present context, the term stable signifies that density increases uniformly in the direction of gravity.

We imagine a plane interface where fluid is saturated with solute, which diffuses into the bulk solvent under the influence of a concentration gradient. If we denote the solute mole fraction by x_1, and distances from the interface measured along a line perpendicular to the interface by ξ, we can write, for the local density,

$$\rho(\xi) = \frac{M_2[1 + x_1(\xi)(M_1/M_2 - 1)]}{\bar{V}_2[1 + x_1(\xi)(\bar{V}_1/\bar{V}_2 - 1)]} \tag{49}$$

where overbars denote partial molar quantities, and 1 and 2 refer to the solute and the solvent, respectively. Away from the interface ($\xi \rightarrow \infty$), we have

$$V(\infty) = V_2(T, P) \tag{50}$$

$$M(\infty) = M_2 \tag{51}$$

$$\rho(\infty) = M_2/V_2 \tag{52}$$

For dilute solutions, we may assume

$$\bar{V}_2 \approx V_2 \neq f(x_1) \tag{53}$$

whereupon the density ratio between interface and bulk becomes

$$\frac{\rho(o)}{\rho(\infty)} = \frac{1 + x_1(o)(M_1/M_2 - 1)}{1 + x_1(o)(\bar{V}_1/V_2 - 1)} \tag{54}$$

from which we conclude

$$\rho(o) > \rho(\infty) \rightleftharpoons (M_1/M_2) > \bar{V}_1/V_2 \tag{55}$$

Because $x_1(o)$ is just a parameter in Eq. 54, it follows that Eq. 55 is a general criterion for the local density of dilute binary systems.

For the full density profile, we write

$$\frac{1}{\rho(\infty)} \cdot \frac{d\rho}{d\xi} = \left(\frac{d\rho}{dx_1} \cdot \frac{dx_1}{d\xi}\right) \cdot \frac{1}{\rho(\infty)} \tag{56}$$

where $dx_1/d\xi$ is a monotonically decreasing function of ξ at steady state. If we now define

$$A = M_1/M_2 - 1 \tag{57}$$

$$B = \bar{V}_1/V_2 - 1 \tag{58}$$

and neglect the composition dependence of B (dilute solutions), we obtain

$$\frac{1}{\rho(\infty)} \cdot \frac{d\rho}{dx_1} = \frac{A - B}{(1 + Bx_1)^2} \tag{59}$$

and we conclude that, for dilute solutions,

$M_1/M_2 > \bar{V}_1/V_2 \rightleftharpoons$ density decreases monotonically away from the interface

$M_1/M_2 < \bar{V}_1/V_2 \rightleftharpoons$ density increases monotonically away from the interface

Schematic profiles are shown in Figure 14. For stable profiles, then, the interface should constitute the bottom of the rectangular duct if the solute to solvent molecular weight ratio exceeds the corresponding partial molar volume ratio. In all of the cases presently considered, stable profiles were developed with the interface at the bottom, and consequently the source plane constituted the bottom of the rectangular duct (Debenedetti, 1984); natural convection was introduced by rotating the hemicylinders away from this equilibrium configuration.

The results of such experiments are shown, for benzoic acid diffusing into CO_2 at 318 K and 160 bar, in Figure 15. The dashed line (mass transfer rate) in this figure does not extend to 0° since the diffusion experiment was done at a different flow rate. The importance of natural convection, as well as the potential for experimental error when using hydrodynamic techniques, can be seen from the fact that a 550% increase in the apparent diffusion coefficient results from a 90° rotation of the flat plate.

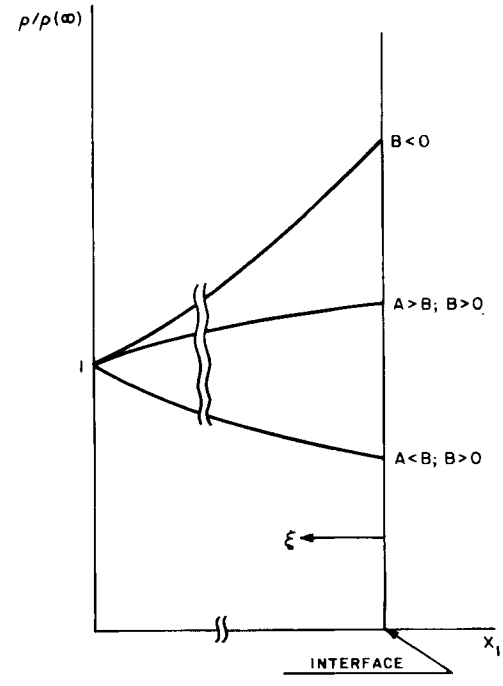

Figure 14. Schematic density profiles for a dilute binary mixture in which a solute dissolves into the solvent from a plane ($\xi = 0$) of constant composition.

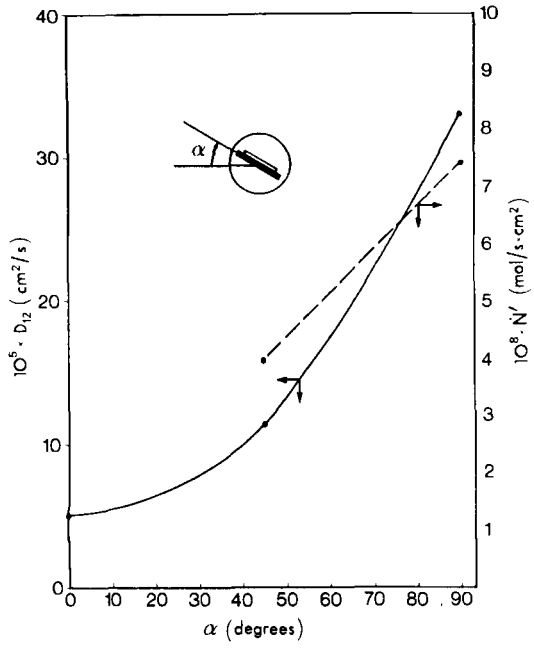

Figure 15. Effect of natural convection on apparent diffusion coefficient and mass transfer rate for benzoic acid–CO_2 system at 318 K, 160 bar.

Conclusions

Significant rate enhancements due to natural convection will result in supercritical extraction processes whenever the controlling resistance to mass transfer is in the supercritical phase. This is a consequence of the unusually low kinematic viscosities of fluids in the near supercritical region, which in turn arise as a result of the different behavior of density and viscosity in going from the dilute gas to the dense fluid region.

True binary diffusion coefficients, as well as mass transfer enhancements due to natural convection can be measured with a hydrodynamic technique whereby experiments can be conducted either in the absence or in the presence of buoyant effects.

Hydrodynamic behavior at the molecular level is approached as a high-density (or -viscosity) limit, and can be used to correlate experimental data. The breakdown of hydrodynamic behavior is currently poorly understood and deserves further attention.

Notation

A = preexponential factor in Andrade expression, $ML^{-1}t^{-1}$; molecular weight factor
A' = z-dependent coefficient
A_n = nth expansion coefficient
a = duct semiwidth (transverse), L; radius of Brownian sphere, L; exponent in Hayduck-Cheng expression
a_j = jth coefficient of homogeneous part of solution to Eq. 32
a'_j = reduced coefficient of homogeneous part of solution to Eq. 32
B = exponential factor in Andrade expression, θ; partial molar volume factor
B_n = nth expansion coefficient
b = duct semiheight (vertical), L
c_{ij} = coefficient for $a'j$ expansion in terms of eigenvalues
c = solute concentration, mol · L^{-3}
$\mathcal{D}$ = diffusion coefficient, L^2t^{-1}
D = duct diameter, L
E_n = nth expansion coefficient
F_n = defined in Eq. A9
g = acceleration due to gravity, L t^{-2}
Gr = Grashof number, $g\ell^3(\Delta\rho/\rho)/\nu^2$
Gz' = modified Graetz number, $x\mathcal{D}/\langle v\rangle b_2$
H = homogeneous part of solution to Eq. 32
h = relative height, L
k = mass transfer coefficient, Lt^{-1}; Boltzmann's constant, $ML^2t^{-2}\theta^{-1}$
L = coated length, L
M_i = molecular weight of species i, M mol^{-1}
m = velocity profile exponent
n = velocity profile exponent
P = pressure, $ML^{-1}t^{-2}$
Pe = Peclet number, $\langle v\rangle L/\mathcal{D}$
R = duct radius, L
r = relative saturation
Ra = Rayleigh number, $g\ell^3(\Delta\rho/\rho)/\nu\mathcal{D}$
Re = Reynolds number, $\langle v\rangle\ell/\nu$
Sc = Schmidt number, $\nu/\mathcal{D}$
Sh = Sherwood number, $k\ell/\mathcal{D}$
s = surface area, L^2
T = temperature, θ
t = time, t
V = molar volume, $L^3 \cdot mol^{-1}$
V_0 = hard sphere close-packed molar volume, $L^3 \cdot mol^{-1}$
v = velocity, Lt^{-1}
x = duct axial coordinate L
x_i = species i mole fraction
y = duct vertical coordinate, L
z = duct transverse coordinate, L

Greek letters

α = duct aspect ratio
β = duct aspect ratio
β_m = defined in Eq. 4, $L^3 \cdot mol^{-1}$
γ_n = nth eigenvalue of Eq. A3
ζ = transformed vertical coordinate, L
η = viscosity, $ML^{-1}t^{-1}$
ν = kinematic viscosity, L^2t^{-1}
ξ = coordinate along direction normal to interface, L
σ = hard sphere diameter, L
ϕ_n = nth integral expansion coefficient
ψ_n = nth integral expansion coefficient
π = modified pressure, Eq. 6, $ML^{-1}t^{-2}$
ρ = density, ML^{-3}

Subscripts

i = interface
r = reduced quantity
o = reference conditions
$\sim$ = vector quantity

Superscripts

$+$ = dimensionless quantity
$-$ = partial molar quantity
o = unit vector

Appendix

$$\phi_n = \int_0^1 (1-\eta^m)\exp\left[\frac{-\dfrac{2m\gamma_n^2}{3(m+1)}\cdot Gz'}{1-\eta^m}\right]d\eta \qquad \text{(A1)}$$

$$\psi_n = \int_0^1 \exp\left[\frac{-\dfrac{2m\gamma_n^2}{3(m+1)}\cdot Gz'}{1-\eta^m}\right]d\eta \qquad \text{(A2)}$$

Equation 32 is solved by variable separation. This leads to a

Table A1. Eigenvalues and Expansion Coefficients

n	A	B	E	γ
1	−0.6242144449211	−0.8717135423055	−0.5970396020662	0.9546676
2	0.1916121727370	1.62136522176	$-0.4033326872425 \times 10^{-1}$	2.9743079
3	−0.1136094212907	−2.606320953153	$-0.1209851681885 \times 10^{-1}$	4.9810344
4	$0.4394766591177 \times 10^{-5}$	196,572.6180829	$0.5196364776233 \times 10^{-2}$	6.9845839
5	$0.3212078027422 \times 10^{-10}$	26,634,903,493.79	$0.4744797120123 \times 10^{-2}$	8.9876252

homogeneous (ζ^+) and a nonhomogeneous (x^+) problem. If the former is series-expanded, there results an eigenvalue problem. γ_n is the nth eigenvalue of the equation

$$H'' + (2\zeta^+ - \zeta^{+2})\gamma^2 H = 0 \tag{A3}$$

where

$$H = \sum_{j=0}^{\infty} a_j \zeta^{+j} \tag{A4}$$

and the recurrence law for the a_j is obtained from Eq. 36, leading to an even power series,

$$a'_i = \frac{a_i}{a_o} = \sum_{j=1}^{\infty} C_{ij} \gamma^{2j} \tag{A5}$$

The coefficients A_n, B_n, E_n in Eqs. 38 and 39 are given by

$$A_n = \int_0^2 \frac{(2\zeta^+ - \zeta^{+2}) F_n}{\gamma_n \left(\dfrac{dF_n}{d\gamma_n}\right)_{(\zeta^+=2)}} d\zeta^+ \tag{A6}$$

$$B_n = \frac{1}{\sum_{k=2}^{\infty} 2^{k+1} \sum_{j=1}^{\infty} j\, C_{kj}\, \gamma_n^{2j}} \tag{A7}$$

$$E_n = \sum_{j=2}^{\infty} j\, 2^{j-1} \sum_{k=1}^{\infty} C_{jk}\, \gamma_n^{2k} \tag{A8}$$

$$F_n = 1 + a'_{1,n}\zeta^+ + a'_{2,n}\zeta^{+2} + \cdots \tag{A9}$$

where $a'_{i,n}$ signifies the quantity in Eq. A5, evaluated with the nth eigenvalue, γ_n.

Table A1 gives the values of the first five eigenvalues and expansion coefficients (γ, A, B, E). To obtain these numbers, it was necessary to use terms up to a_{80} (Eq. A4), γ^{52} (Eq. A5), and hence $C_{80,26}$. These upper limits were used in the sums of Eqs. A7 and A8.

Literature cited

Allen, G., J. G. Watkinson, and K. H. Webb, "An Infrared Study of Benzoic Acid in the Vapor Phase, and in Dilute Solution in Nonpolar Solvents," *Spectroch. Acta.* **22,** 807, (1966).

Andrade, E. N. daC., "The Viscosity of Liquids," *Nature,* **125,** 309 (1930).

Angus, S., B. Armstrong, and K. M. de Reuck, *Carbon Dioxide—International Thermodynamic Tables of the Fluid State,* **3** (IUPAC), Pergamon, Oxford (1976).

Chandler, D., "Rough Hard Sphere Theory of the Self-Diffusion Constant for Molecular Liquids," *J. Chem. Phys.,* **62**(4), 1358 (1975).

Chapman, S., and T. G. Cowling, *The Mathematical Theory of Nonuniform Gases,* Cambridge Univ. Press (1970).

Chen, S., "A Rough Hard Sphere Theory for Diffusion in Supercritical Carbon Dioxide," *Chem. Eng. Sci.,* **38**(4), 655 (1983).

Debenedetti, P. G., "Diffusion and Mass Transfer in Supercritical Fluids," Ph.D. Thesis, Massachusetts Inst. Tech. (1984).

Dymond, J. H., "Corrected Enskog Theory and the Transport Coefficients of Liquids," *J. Chem. Phys.,* **60**(3), 969 (1974).

Eckert, E. R. G., and R. M. Drake, *Analysis of Heat and Mass Transfer,* McGraw-Hill, New York (1972).

Feist, R., and G. M. Schneider, "Determination of Binary Diffusion Coefficients of Benzene, Phenol, Naphthalene and Caffeine in Supercritical CO_2 between 308 and 333K in the Pressure Range 80 to 160 bar with Supercritical Fluid Chromatography (SFC)," *Sep. Sci. Tech.,* **17**(1), 261 (1982).

Fury, M., G. Munie, and J. Jonas, "Transport Processes in Compressed Liquid Pyridine," *J. Chem. Phys.,* **70**(3), 1260 (1979).

Hayduk, W., and S. C. Cheng, "Review of Relation between Diffusivity and Solvent Viscosity in Dilute Liquid Solutions," *Chem. Eng. Sci.,* **26,** 635 (1971).

I'Haya, Y., and T. Shibuya, "The Dimerization of Benzoic Acid in Carbon Tetrachloride and Chloroform," *Bull. Chem. Soc. Japan,* **38**(7), 1144 (1965).

Iomtev, M. B., and Y. V. Tsekhanskaya, "Diffusion of Naphthalene in Compressed Ethylene and Carbon Dioxide," *Russ. J. Phys. Chem.,* **38**(4), 485 (1964).

Jossi, J. A., L. I. Stiel, and G. Thodos, "The Viscosity of Pure Substances in the Dense Gaseous and Liquid Phases," *AIChE J.,* **8**(1), 59 (1962).

Karabelas, A. J., T. H. Wegner, and T. J. Hanratty, "Use of Asymptotic Relations to Correlate Mass Transfer Data in Packed Beds," *Chem. Eng. Sci.,* **26,** 1581 (1971).

Kurnik, R. T., "Supercritical Extraction: A Study of Binary and Multicomponent Solid-Fluid Equilibria," Sc.D. Thesis, Massachusetts Inst. Tech. (1981).

Kurnik, R. T., S. J. Holla, and R. C. Reid, "Solubility of Solids in Supercritical Carbon Dioxide and Ethylene," *J. Chem. Eng. Data,* **26,** 47 (1981).

Kurnik, R. T., and R. C. Reid, "Solubility Extrema in Solid-Fluid Equilibria," *AIChE J.,* **27,** 861 (1981).

Lusis, M. A., and G. A. Ratcliff, "Diffusion in Binary Liquid Mixtures at Infinite Dilution," *Can. J. Chem. Eng.,* **46,** 385 (1968).

Metais, B., and E. R. G. Eckert, "Forced, Mixed, and Free Convection Regimes," *J. Heat Transf.,* **86,** 295 (1964).

Paulaitis, M. E., V. J. Krukonis, R. T. Kurnik, and R. C. Reid, "Supercritical Fluid Extraction," *Rev. in Chem. Eng.,* **1**(2), 179 (1983).

Peng, D. Y., and D. B. Robinson, "A New Two-Constant Equation of State," *Ind. Eng. Chem. Fundam.,* **15,** 59 (1976).

Reddy, K. A., and L. K. Doraiswamy, "Estimating Liquid Diffusivity," *Ind. Eng. Chem. Fundam.,* **6**(1), 77 (1967).

Reid, R. C., J. M. Prausnitz, and T. K. Sherwood, *The Properties of Gases and Liquids,* 3rd ed., McGraw-Hill, New York (1977).

Scheibel, E. G., "Liquid Diffusivities," *Ind. Eng. Chem.,* **46**(9), 2007 (1954).

Schmitt, W. J., and R. C. Reid, "The Solubility of Monofunctional Organic Solids in Chemically Diverse Supercritical Fluids," *J. Chem. Eng. Data* **31,** 204 (1986).

Shah, R. K., and A. L. London, *Laminar Flow Forced Convection in Ducts,* Academic Press, New York (1978).

Swaid, I., and G. M. Schneider, "Determination of Binary Diffusion Coefficients of Benzene and Some Alkylbenzenes in Supercritical CO_2 between 308 and 328 K in the Pressure Range 80 to 160 bar with

Supercritical Fluid Chromatography," *Ber. Bunsenges. Phys. Chem.*, **83**, 969 (1979).
Wilke, C. R., and P. Chang, "Correlations of Diffusion Coefficients in Dilute Solutions," *AIChE J.*, **1**(2), 264 (1955).

Manuscript received Feb. 3, 1986, and revision received May 5, 1986.

See NAPS document no. 04433 for 5 pages of supplementary material. Order from NAPS c/o Microfiche Publications, P.O. Box 3513, Grand Central Station, New York, NY 10163. Remit in advance in U.S. funds only $7.75 for photocopies or $4.00 for microfiche. Outside the U.S. and Canada, add postage of $4.50 for the first 20 pages and $1.00 for each of 10 pages of material thereafter, $1.50 for microfiche postage.